

Supplemental Material for Vertex corrections to conductivity in the Holstein model: A numerical–analytical study

Veljko Janković,* Petar Mitrić,† Darko Tanasković,‡ and Nenad Vukmirović§
Institute of Physics Belgrade, University of Belgrade, Pregrevica 118, 11080 Belgrade, Serbia

SI. HEOM

For the sake of completeness, here, we present the equations that we solve to obtain numerically exact and bubble-approximation results for the current–current correlation function and the dynamical-mobility profile.

A. Dynamical equations of the HEOM for $C_{jj}(t)$

As we have discussed in Ref. 1, the totally symmetric ($q = 0$) phonon mode does not affect the dynamics of $C_{jj} = \text{Tr}_e\{j\iota(t)\}$, which follows from the evolution of the purely electronic operator

$$\iota(t) = Z^{-1} \text{Tr}_{\text{ph}}\{e^{-iHt} j e^{-\beta H} e^{iHt}\} \quad (\text{S1})$$

The operator $\iota(t)$ is at the root of the hierarchy of dynamical equations, whose higher-order members $\iota_{\mathbf{n}}^{(n)}(t)$ describe the dynamics of n -phonon assisted processes determined by the vector $\mathbf{n} = \{n_{qm} | q \neq 0; m = 0, 1\}$ of non-negative integers n_{qm} that obey $\sum'_{qm} n_{qm} = n$. The total momentum exchanged between the electron and phonons in the phonon-assisted process described by \mathbf{n} is $k_{\mathbf{n}} = \sum'_{qm} q n_{qm}$. In the following, primed sums over q exclude the $q = 0$ term. By virtue of the translational symmetry, the only non-zero matrix elements of $\iota_{\mathbf{n}}^{(n)}(t)$ are $\langle k | \iota_{\mathbf{n}}^{(n)}(t) | k + k_{\mathbf{n}} \rangle$, and their time evolution is governed by

$$\begin{aligned} \partial_t \langle k | \iota_{\mathbf{n}}^{(n)}(t) | k + k_{\mathbf{n}} \rangle = & \\ & - i(\varepsilon_k - \varepsilon_{k+k_{\mathbf{n}}} + \mu_{\mathbf{n}}) \langle k | \iota_{\mathbf{n}}^{(n)}(t) | k + k_{\mathbf{n}} \rangle \\ & + i \sum'_{qm} \sqrt{(1 + n_{qm}) c_m} \langle k - q | \iota_{\mathbf{n}_{qm}^+}^{(n+1)}(t) | k + k_{\mathbf{n}} \rangle \\ & - i \sum'_{qm} \sqrt{(1 + n_{qm}) c_m} \langle k | \iota_{\mathbf{n}_{qm}^+}^{(n+1)}(t) | k + k_{\mathbf{n}} + q \rangle \\ & + i \sum'_{qm} \sqrt{n_{qm} c_m} \langle k + q | \iota_{\mathbf{n}_{qm}^-}^{(n-1)}(t) | k + k_{\mathbf{n}} \rangle \\ & - i \sum'_{qm} \sqrt{n_{qm} \frac{c_m}{\sqrt{c_m}}} \langle k | \iota_{\mathbf{n}_{qm}^-}^{(n-1)}(t) | k + k_{\mathbf{n}} - q \rangle \\ & + \left[\partial_t \langle k | \iota_{\mathbf{n}}^{(n)}(t) | k + k_{\mathbf{n}} \rangle \right]_{\text{close}}. \end{aligned} \quad (\text{S2})$$

In Eq. (S2), $\mu_{\mathbf{n}} = \omega_0 \sum'_q (n_{q0} - n_{q1})$. The operator $\iota_{\mathbf{n}}^{(n)}(t)$ couples to analogous operators at depths $n \pm 1$, which are characterized by vectors \mathbf{n}_{qm}^{\pm} whose components are $[\mathbf{n}_{qm}^{\pm}]_{q'm'} = n_{q'm'} \pm \delta_{q'q} \delta_{m'm}$. The coefficients c_m are defined in Eqs. (A8) and (A9) of Appendix A. The last term on the right-hand side of Eq. (S2) represents the closing term,

* veljko.jankovic@ipb.ac.rs

† petar.mitric@ipb.ac.rs

‡ darko.tanaskovic@ipb.ac.rs

§ nenad.vukmirovic@ipb.ac.rs

which renders the HEOM truncated at the maximum depth D numerically stable. In Ref. 1, we have checked that the following closing term

$$\begin{aligned} & \left[\partial_t \langle k | \rho_{\mathbf{n}}^{(n)}(t) | k + k_{\mathbf{n}} \rangle \right]_{\text{close}} = \\ & - \delta_{n,D} \frac{1}{2} (\tau_k^{-1} + \tau_{k+k_{\mathbf{n}}}^{-1}) \langle k | \rho_{\mathbf{n}}^{(n)}(t) | k + k_{\mathbf{n}} \rangle \end{aligned} \quad (\text{S3})$$

stabilizes the HEOM in Eq. (S2) without compromising final results for the dynamical-mobility profile. The closing term comprises the rates at which the electron is scattered out of the free-electron state $|k\rangle$

$$\begin{aligned} \tau_k^{-1} = 2\pi \frac{g^2}{N} \sum_q' & [(1 + n_{\text{ph}}) \delta(\varepsilon_k - \varepsilon_{k-q} - \omega_0) \\ & + n_{\text{ph}} \delta(\varepsilon_k - \varepsilon_{k-q} + \omega_0)], \end{aligned} \quad (\text{S4})$$

which can be computed analytically in the limit $N \rightarrow \infty$.

B. Dynamical equations of the HEOM for $G^{\geq}(k, t)$

The dynamics of the current-current correlation function in the bubble approximation follows from the dynamics of $G^>(k, t)$ and $G^<(k, t)$ as defined in Eqs. (A13) and (A14) of Appendix A. Both quantities can be computed by solving the same set of dynamical equations that have been presented in Ref. 2 and read as

$$\begin{aligned} & \partial_t G_{\mathbf{n}}^{(\geq, n)}(k - k_{\mathbf{n}}, t) = \\ & - i(\varepsilon_{k-k_{\mathbf{n}}} + \mu_{\mathbf{n}}) G_{\mathbf{n}}^{(\geq, n)}(k - k_{\mathbf{n}}, t) \\ & + i \sum_{qm}' \sqrt{1 + n_{qm}} \sqrt{c_m} G_{\mathbf{n}_{qm}^+}^{(\geq, n+1)}(k - k_{\mathbf{n}} - q, t) \\ & + i \sum_{qm}' \sqrt{n_{qm}} \sqrt{c_m} G_{\mathbf{n}_{qm}^-}^{(\geq, n-1)}(k - k_{\mathbf{n}} + q, t) \\ & + [\partial_t G_{\mathbf{n}}^{(\geq, n)}(k - k_{\mathbf{n}}, t)]_{\text{close}}. \end{aligned} \quad (\text{S5})$$

To ensure that G^{\geq} decays to zero at sufficiently long times, we use the closing term $[\partial_t G_{\mathbf{n}}^{(\geq, n)}(k - k_{\mathbf{n}}, t)]_{\text{close}}$. Its form after truncation of Eq. (S5) at the maximum depth D can be derived along the lines presented in Ref. 1. The final expression for the closing term is analogous to that presented in Eq. (S3) and reads as

$$\begin{aligned} & [\partial_t G_{\mathbf{n}}^{(\geq, n)}(k - k_{\mathbf{n}}, t)]_{\text{close}} = \\ & - \delta_{n,D} \frac{1}{2} \tau_{k-k_{\mathbf{n}}}^{-1} G_{\mathbf{n}}^{(\geq, n)}(k - k_{\mathbf{n}}, t), \end{aligned} \quad (\text{S6})$$

where τ_k is defined in Eq. (S4).

The propagation of Eq. (S5) is additionally stabilized by transferring to the rotating-wave frame and solving equations for the envelope $\tilde{G}_{\mathbf{n}}^{(\geq, n)}(t)$ defined as

$$\begin{aligned} G_{\mathbf{n}}^{(\geq, n)}(k - k_{\mathbf{n}}, t) = \exp[-i(\varepsilon_{k-k_{\mathbf{n}}} + \mu_{\mathbf{n}})t] \times \\ \tilde{G}_{\mathbf{n}}^{(\geq, n)}(k - k_{\mathbf{n}}, t). \end{aligned} \quad (\text{S7})$$

We note that the HEOM in Eq. (S5) has a smaller number of equations than the HEOM we solved in Ref. 2. This reduction in HEOM size is possible because the part of the dynamics governed by the zero-momentum phonon mode can be solved analytically. Additionally, this implies $G^{\geq}(k, t) \neq G_0^{(\geq, 0)}(k, t)$, and we now establish the relationship between the quantity of our interest $G^{\geq}(k, t)$ and the quantity at the root of the hierarchy $G_0^{(\geq, 0)}(k, t)$. The $q = 0$ phonon mode couples to the unit operator in the subspace containing a single electron, i.e., $V_{q=0} = \mathbb{1}_{1e}$, meaning that the action of the corresponding $q = 0$ components of the influence phases $\varphi_1(t)$ and $\varphi_3(t, \beta)$ [see Eqs. (A16) and (A18) of Appendix A] can be evaluated analytically. The analytical procedure is, up to prefactors N^{-1} , identical to

that presented in Sec. SII, and produces the following final results for $G^{\gtrless}(k, t)$:

$$\begin{aligned}
G^>(k, t) &= \tilde{G}_{\mathbf{0}}^{(>,0)}(k, t)e^{-i\varepsilon_k t} \\
&\times \exp \left[-\sum_m c_m \frac{e^{-\mu_m t} + \mu_m t - 1}{\mu_m^2} \right] \\
&= \tilde{G}_{\mathbf{0}}^{(>,0)}(k, t)e^{-i\varepsilon_k t} \exp \left[-\frac{g^2}{\omega_0^2 N} (1 + 2n_{\text{ph}}) \right] \\
&\times \exp \left[\frac{g^2}{\omega_0^2 N} \left((1 + n_{\text{ph}})e^{-i\omega_0 t} + n_{\text{ph}}e^{i\omega_0 t} + i\omega_0 t \right) \right],
\end{aligned} \tag{S8}$$

$$\begin{aligned}
G^<(k, t) &= \tilde{G}_{\mathbf{0}}^{(<,0)}(k, t)e^{-i\varepsilon_k t} \\
&\times \exp \left[-\sum_m \frac{c_m}{\mu_m^2} (e^{-\mu_m t} + \mu_m t - 1) \right] \\
&\times \exp \left[\sum_m \frac{c_m}{\mu_m^2} (e^{-\mu_m t} - 1)(1 - e^{i\beta\mu_m}) \right] \\
&= \tilde{G}_{\mathbf{0}}^{(<,0)}(k, t)e^{-i\varepsilon_k t} \exp \left[-\frac{g^2}{\omega_0^2 N} (1 + 2n_{\text{ph}}) \right] \\
&\times \exp \left[\frac{g^2}{\omega_0^2 N} \left(n_{\text{ph}}e^{-i\omega_0 t} + (1 + n_{\text{ph}})e^{i\omega_0 t} + i\omega_0 t \right) \right].
\end{aligned} \tag{S9}$$

C. Initial conditions

The initial condition under which the HEOM for $G^>$ [Eq. (S5)] is solved reads as [2]

$$G_{\mathbf{n}}^{(>,n)}(k - k_{\mathbf{n}}, 0) = -i\delta_{n,0}. \tag{S10}$$

The initial conditions under which the HEOM for $\iota(t)$ [Eq. (S2)] and $G^<$ [Eq. (S5)] is solved is determined by the equilibrium state of the interacting electron-phonon system [1, 2]. In Ref. 2, we derived that the hierarchical representation of this state is obtained by propagating the following imaginary-time HEOM:

$$\begin{aligned}
&\partial_{\tau} \langle k | \sigma_{\mathbf{n}}^{(n)}(\tau) | k + k_{\mathbf{n}} \rangle = \\
&- (\varepsilon_k + \mu_{\mathbf{n}}) \langle k | \sigma_{\mathbf{n}}^{(n)}(\tau) | k + k_{\mathbf{n}} \rangle \\
&+ \sum_{qm}' \sqrt{(1 + n_{qm})} c_m \langle k - q | \sigma_{\mathbf{n}_{qm}^+}^{(n+1)}(\tau) | k + k_{\mathbf{n}} \rangle \\
&+ \sum_{qm}' \sqrt{n_{qm}} c_m \langle k + q | \sigma_{\mathbf{n}_{qm}^-}^{(n-1)}(\tau) | k + k_{\mathbf{n}} \rangle.
\end{aligned} \tag{S11}$$

Equations (S11) are propagated from $\tau = 0$ to $\tau = \beta$ with the initial condition $\langle k | \sigma_{\mathbf{n}}^{(n)}(\tau) | k + k_{\mathbf{n}} \rangle = \delta_{n,0}$, which is representative of the electron-phonon system at infinite temperature. The initial condition for the propagation of Eq. (S2) then reads as

$$\begin{aligned}
\langle k | \iota_{\mathbf{n}}^{(n)}(0) | k + k_{\mathbf{n}} \rangle &= Z_e^{-1} \times \\
(-2J) \sin(k) \langle k | \sigma_{\mathbf{n}}^{(n)}(\beta) | k + k_{\mathbf{n}} \rangle,
\end{aligned} \tag{S12}$$

while the initial condition for the propagation of Eq. (S5) governing the dynamics of $G^<$ is

$$G_{\mathbf{n}}^{(<,n)}(k - k_{\mathbf{n}}, 0) = Z_e^{-1} \times i \langle k | \sigma_{\mathbf{n}}^{(n)}(\beta) | k + k_{\mathbf{n}} \rangle. \tag{S13}$$

The so-called electronic partition sum $Z_e = Z/Z_{\text{ph}}$ entering Eqs. (S12) and (S13) reads as

$$Z_e = \sum_p \langle p | \sigma_{\mathbf{0}}^{(0)}(\beta) | p \rangle. \tag{S14}$$

D. Propagation algorithm

The HEOM embodied in Eq. (S2) is propagated using the scheme originally proposed in Ref. 3. We use the fourth-order Wilkins–Dattani scheme with the time step $\omega_0\Delta t = (1 - 2) \times 10^{-2}$, depending on the values of model parameters.

When the HEOM embodied in Eq. (S5) is recast as the HEOM for the envelope \tilde{G}^{\approx} [Eq. (S7)], it becomes a system of first-order linear differential equations with time-dependent coefficients. Because of its non-constant coefficients, the resulting HEOM for the envelope is propagated using the fourth-order Runge–Kutta algorithm [4] with the time step $\omega_0\Delta t = (1 - 2) \times 10^{-2}$, depending on the values of model parameters.

SII. VANISHING VERTEX CORRECTIONS IN THE LIMIT $t_0 \rightarrow 0$: INSIGHTS FROM FORMALLY EXACT EXPRESSIONS

Starting from the formally exact expressions of Appendix A, this section presents the proof of the equality $C_{jj}(t) = C_{jj}^{\text{bbl}}(t)$ in the limit $t_0 \rightarrow 0$.

As argued in the main text, the dominant term in the expansion of $C_{jj}(t)$ and $C_{jj}^{\text{bbl}}(t)$ in powers of small t_0 is proportional to t_0^2 . This term can be obtained from the formally exact expressions by replacing all operators $e^{-\alpha H_e}$ by the unit operator $\mathbb{1}_{1e}$ in the subspace containing a single electron. In particular, this means that all the real-time/imaginary-time hyperoperators entering the expressions for influence phases become time-independent, which makes the time-ordering sign ineffective and permits us to perform the real-time and/or imaginary-time integrals and sums over q analytically.

Let us first consider how these simplifications are reflected in the influence phases $\varphi_1(t)$, $\varphi_2(\beta)$, and $\varphi_3(t, \beta)$ governing the single-particle dynamics. The phase $\varphi_1(t)$ [Eq. (A16) of Appendix A] simplifies to

$$\varphi_1(t) = \left[\sum_q V_q^C V_{-q}^C \right] \left[\sum_m \frac{c_m}{\mu_m^2} (e^{-\mu_m t} + \mu_m t - 1) \right]. \quad (\text{S15})$$

Because of $V_q V_{-q} = \mathbb{1}_{1e}$, we can replace sum over q by N , meaning that $\varphi_1(t)$ acts as a scalar that reads as

$$\varphi_1(t) = -\frac{g^2}{\omega_0^2} \times \left[(1 + n_{\text{ph}})e^{-i\omega_0 t} + n_{\text{ph}}e^{i\omega_0 t} + i\omega_0 t - (1 + 2n_{\text{ph}}) \right]. \quad (\text{S16})$$

In the same vein,

$$\varphi_2(t) = \beta \frac{g^2}{\omega_0}, \quad (\text{S17})$$

while

$$Z_e = N e^{-\beta g^2 / \omega_0}, \quad (\text{S18})$$

where the factor N comes from the trace of the unit matrix that replaces the operator $e^{-\beta H_e}$ in Eq. (A12) of Appendix A. We thus see that the action of $\varphi_2(\beta)$ is cancelled by the normalization Z_e . The result for $\varphi_3(t, \beta)$ reads as

$$\varphi_3(t, \beta) = \left[\sum_q V_q^C V_{-q}^C \right] \left[\sum_m \frac{c_m}{\mu_m^2} (e^{-\mu_m t} - 1)(e^{i\beta\mu_m} - 1) \right]. \quad (\text{S19})$$

Since $\varphi_3(t, \beta)$ acts on the unit operator in Eq. (A14) of Appendix A, it effectively acts as a scalar ($V_q \mathbb{1}_{1e} V_{-q} = V_q V_{-q} = \mathbb{1}_{1e}$) whose value reads as

$$\varphi_3(t, \beta) = \frac{g^2}{\omega_0^2} (e^{-i\omega_0 t} - e^{i\omega_0 t}). \quad (\text{S20})$$

We finally obtain

$$C_{jj}^{\text{bbl}}(t) = \frac{1}{N} \sum_k j_k^2 e^{-\varphi_1(t) - \varphi_1(t)^* - \varphi_3(t, \beta)^*}. \quad (\text{S21})$$

Since the terms in the exponent do not depend on k , one uses

$$N^{-1} \sum_k j_k^2 = N^{-1} \text{Tr}_e \{j^2\} = 2t_0^2 \quad (\text{S22})$$

to finally arrive at

$$C_{jj}^{\text{bb1}}(t) = 2t_0^2 e^{-\varphi_1(t) - \varphi_1(t)^* - \varphi_3(t, \beta)^*}. \quad (\text{S23})$$

We now turn to $C_{jj}(t)$, starting from

$$\begin{aligned} \Phi_1(t) = & \frac{g^2}{\omega_0^2} \coth\left(\frac{\beta\omega_0}{2}\right) [1 - \cos(\omega_0 t)] \left(\frac{1}{N} \sum_q V_q^\times V_{-q}^\times\right) + \\ & \frac{g^2}{\omega_0^2} [\sin(\omega_0 t) - i\omega_0 t] \left(\frac{1}{N} \sum_q V_q^\times V_{-q}^\circ\right). \end{aligned} \quad (\text{S24})$$

The action of the hyperoperator $\frac{1}{N} \sum_q V_q^\times V_{-q}^\times$ on the current operator j reduces to

$$\frac{1}{N} \sum_q V_q^\times V_{-q}^\times j = 2j \quad (\text{S25})$$

because of

$$\frac{1}{N} \sum_q V_q j V_{-q} = \frac{1}{N} \sum_{qp} j_{p-q} |p\rangle \langle p| = 0, \quad (\text{S26})$$

which follows from $N^{-1} \sum_q e^{iq} = 0$ (under PBCs). In other words, one can replace $\frac{1}{N} \sum_q V_q^\times V_{-q}^\times$ by 2 in Eq. (S24). Along the same line, we conclude that $\frac{1}{N} \sum_q V_q^\times V_{-q}^\circ$ can be replaced by 0 in Eq. (S24). We can thus replace the original $\Phi_1(t)$ by the scalar that reads as

$$\Phi_1(t) = \frac{g^2}{\omega_0^2} (2n_{\text{ph}} + 1) [2 - e^{i\omega_0 t} - e^{-i\omega_0 t}]. \quad (\text{S27})$$

In a similar manner,

$$\Phi_3(t, \beta) = -2 \frac{g^2}{\omega_0^2} i \sin(\omega_0 t) \left(\frac{1}{N} \sum_q V_q^\times {}^C V_{-q}\right). \quad (\text{S28})$$

Using the same reasoning as above, we find that

$$\frac{1}{N} \sum_q V_q^\times {}^C V_{-q} j = -j, \quad (\text{S29})$$

so that the influence phase $\Phi_3(t, \beta)$ effectively acts as the following scalar:

$$\Phi_3(t, \beta) = \frac{g^2}{\omega_0^2} (e^{i\omega_0 t} - e^{-i\omega_0 t}). \quad (\text{S30})$$

Collecting all pieces together, we remain with

$$C_{jj}(t) = \frac{1}{N} \text{Tr}_e \{j^2\} e^{-\Phi_1(t) - \Phi_3(t, \beta)}. \quad (\text{S31})$$

The equality $C_{jj}(t) = C_{jj}^{\text{bb1}}(t)$ then follows from Eqs. (S16), (S20), (S27), and (S30).

SIII. SUMMARY OF THE PARAMETER REGIMES EXAMINED

Method ($\omega_0/t_0, \lambda$)	HEOM	QMC	HEOM bubble	QMC bubble	DMFT
$(1, \frac{1}{100})$	[1, 10]	[1, 10]	[1, 10]	[1, 10]	[1, 10]
$(1, \frac{1}{8})$	[1, 10]	[1, 10]	[1, 10]	[1, 10]	[1, 10]
$(1, \frac{1}{2})$	[0.4, 10]	[0.2, 10]	[0.4, 10]	[0.2, 10]	[0.2, 10]
(1, 1)	[2, 10]	[1, 10]	[2, 10]	[1, 10]	[1, 10]
(1, 2)	×	[1, 10]	×	[1, 10]	[1, 10]
$(\frac{1}{3}, \frac{1}{100})$	[1, 10]	[1, 10]	[1, 10]	[1, 10]	[1, 10]
$(\frac{1}{3}, \frac{1}{8})$	[1, 10]	[1, 10]	[1, 10]	[1, 10]	[1, 10]
$(\frac{1}{3}, \frac{1}{2})$	[1, 10]	[0.1, 10]	[1, 10]	[0.1, 10]	[0.1, 10]
$(\frac{1}{3}, 1)$	[1, 5]	[1, 10]	[1, 5]	[1, 10]	[1, 10]
$(\frac{1}{3}, 2)$	×	[1, 10]	×	[1, 10]	[1, 10]
$(3, \frac{1}{8})$	[5, 10]	[2, 10]	[5, 10]	[2, 10]	[2, 10]
$(3, \frac{1}{2})$	[2, 10]	[1, 10]	[2, 10]	[1, 10]	[1, 10]
(3, 1)	[2, 10]	[1, 10]	[2, 10]	[1, 10]	[1, 10]
(3, 2)	×	[1, 10]	×	[1, 10]	[1, 10]

TABLE S1. Summary of parameter regimes [determined by pairs $(\omega_0/t_0, \lambda)$] and numerical methods that are used to assess the importance of vertex corrections. For each parameter regime and each method, we provide the minimum (T_{\min}/t_0) and maximum (T_{\max}/t_0) temperature at which we performed computations. The choice of parameter values is largely dictated by the feasibility of HEOM and HEOM bubble computations. We emphasize that the DMFT results for the dynamical mobility are available for all values of $\omega_0/t_0, \lambda$, and T , and the same applies to QMC and QMC bubble results for short-time dynamics of C_{jj} . For $\lambda = 2$, HEOM and HEOM bubble computations could be performed only on short time scales [comparable to those accessible by QMC (bubble), see also Sec. III.F of Ref. 1], which is indicated by "×".

SIV. EXTENSIVE COMPARISONS OF HEOM AND DMFT RESULTS

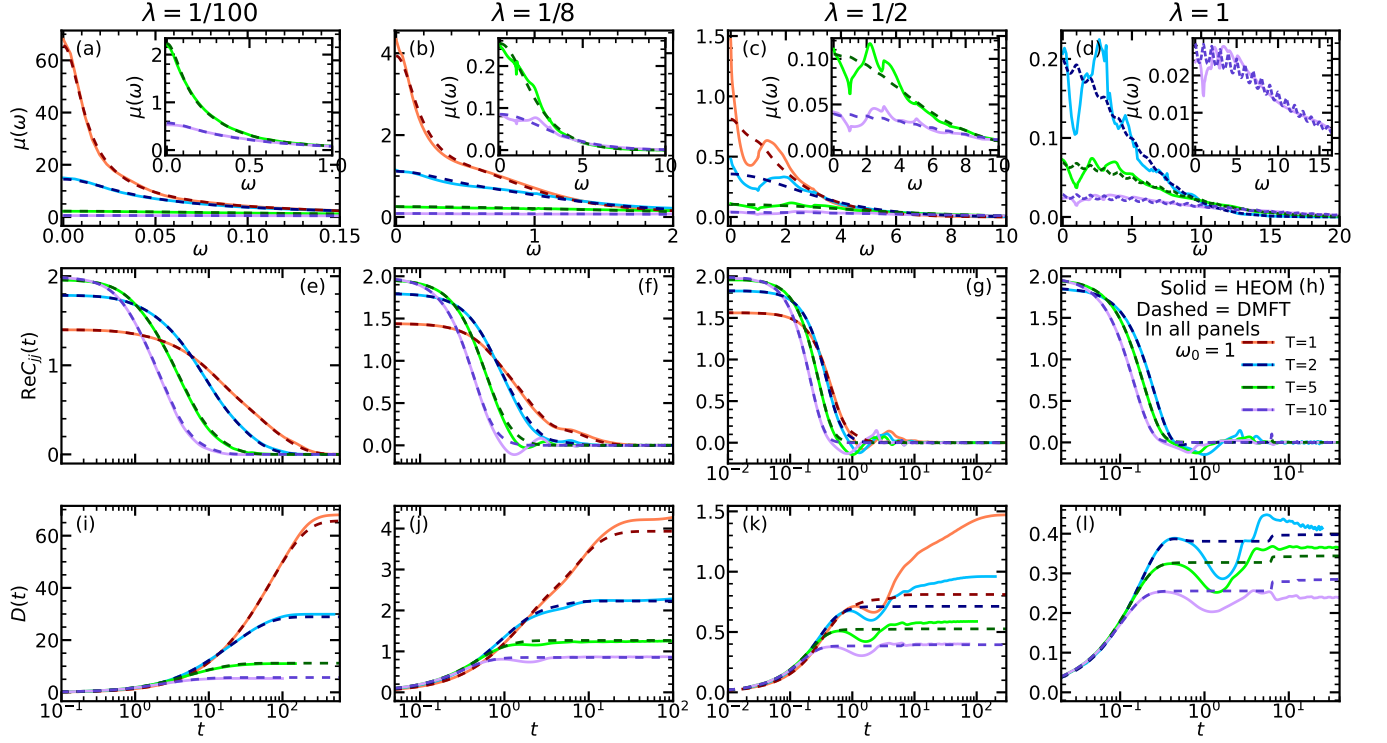
A. Intermediate-frequency phonons ($\omega_0/t_0 = 1$)

FIG. S1. Comparison of HEOM (solid lines) and DMFT (dashed lines) results for (a)–(d) the dynamical-mobility profile, (e)–(h) the real part of the current–current correlation function $C_{jj}(t)$, and (i)–(l) the diffusion constant $\mathcal{D}(t)$. In all panels, $t_0 = \omega_0 = 1$. The strength of the electron–phonon interaction is determined by the cited values of λ , while the temperatures are $T = 1, 2, 5$, and 10 . The insets in panels (a)–(d) zoom in the dynamical-mobility profiles for the highest temperatures considered ($T = 5$ and 10).

B. Slow phonons ($\omega_0/t_0 = 1/3$)

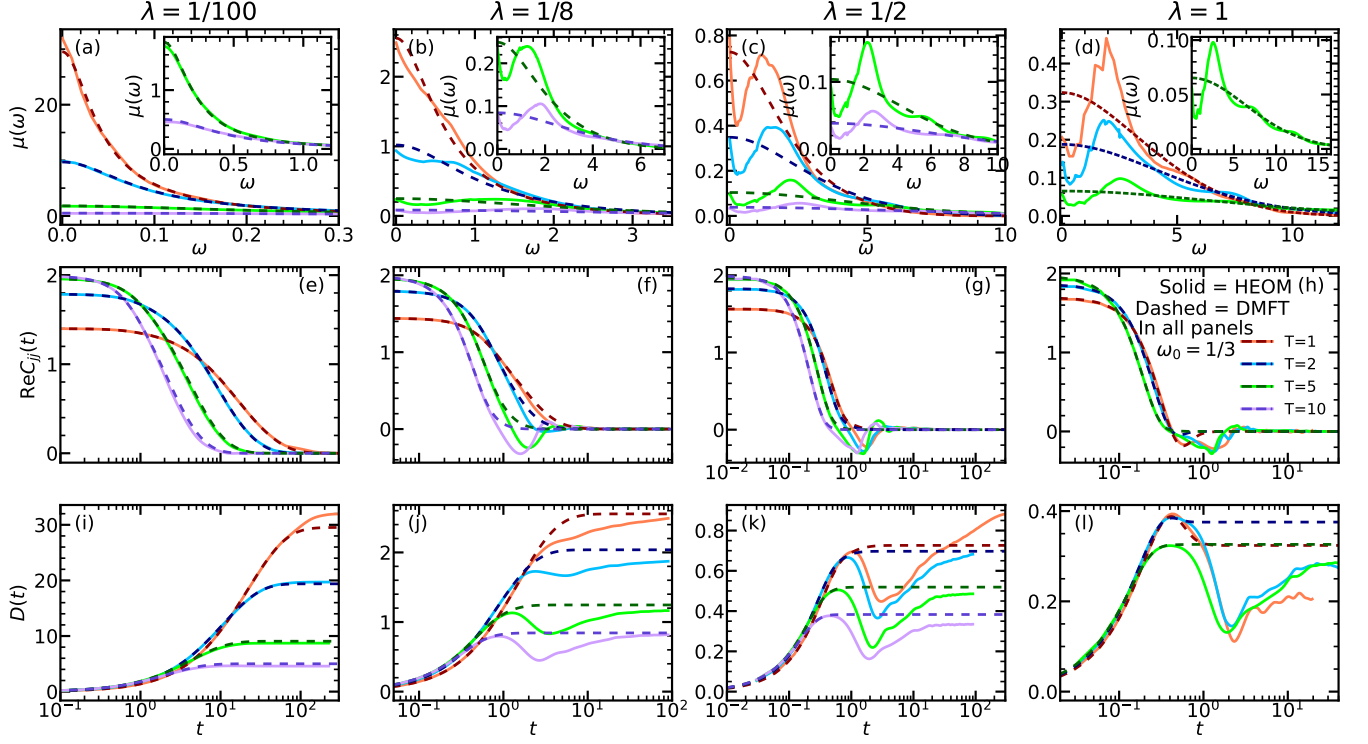


FIG. S2. Comparison of HEOM (solid lines) and DMFT (dashed lines) results for (a)–(d) the dynamical-mobility profile, (e)–(h) the real part of the current–current correlation function $C_{jj}(t)$, and (i)–(l) the diffusion constant $\mathcal{D}(t)$. In all panels, $t_0 = 1, \omega_0 = 1/3$. The strength of the electron–phonon interaction is determined by the cited values of λ , while the temperatures are $T = 1, 2, 5$, and 10 . The insets in panels (a)–(d) zoom in the dynamical-mobility profiles for the highest temperatures considered ($T = 5$ and 10).

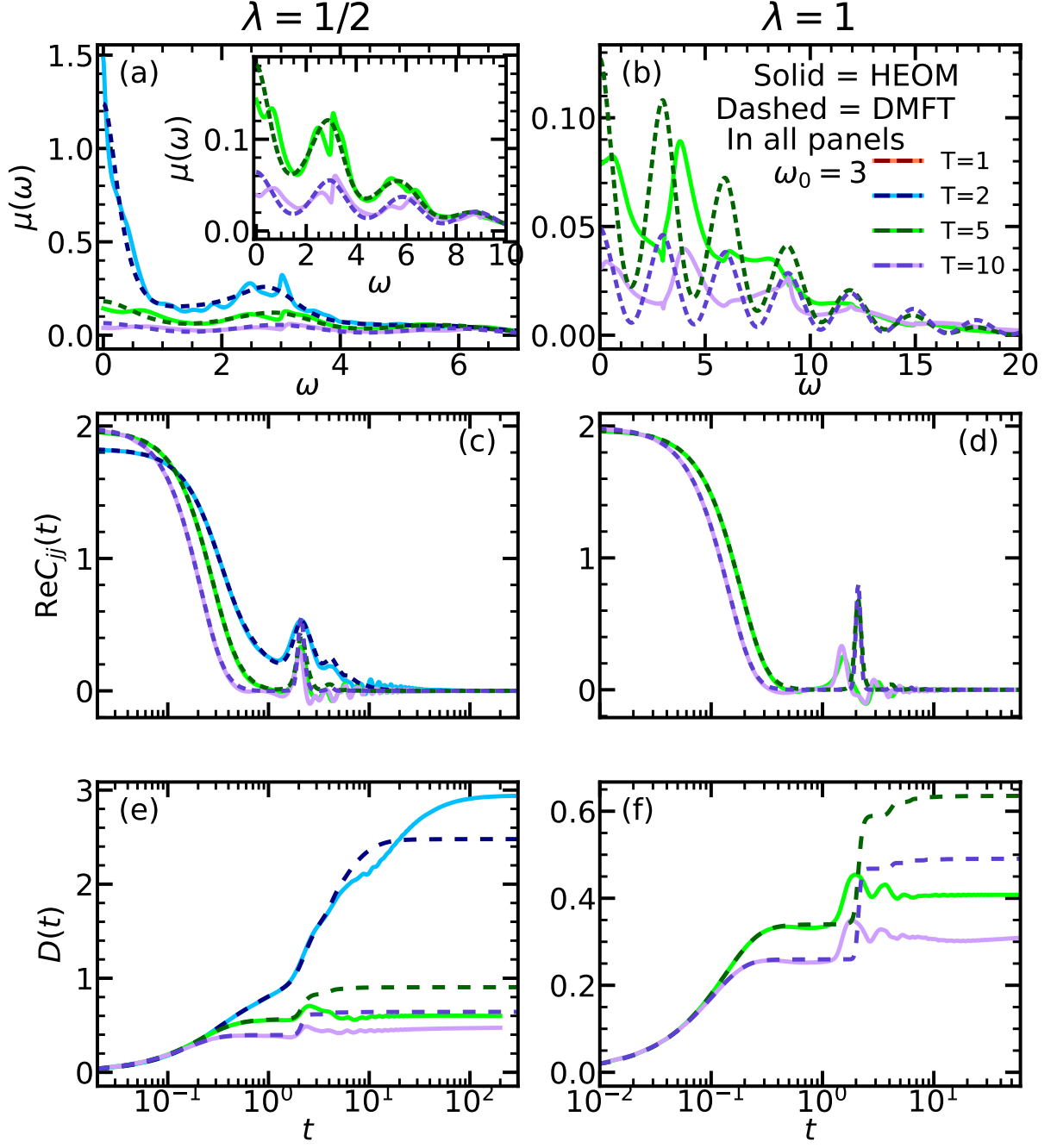
C. Fast phonons ($\omega_0/t_0 = 3$)

FIG. S3. Comparison of HEOM (solid lines) and DMFT (dashed lines) results for (a) and (b) the dynamical-mobility profile, (c) and (d) the real part of the current-current correlation function $C_{jj}(t)$, and (e) and (f) the diffusion constant $\mathcal{D}(t)$. In all panels, $t_0 = 1, \omega_0 = 3$. The strength of the electron-phonon interaction is determined by the cited values of λ , while the temperatures are $T = 2, 5$, and 10 . The inset in panel (a) zooms in the dynamical-mobility profile for the highest temperatures considered ($T = 5$ and 10).

SV. REAL-TIME QMC IN THE LIMIT $\omega_0 \rightarrow 0$

Phonon momentum can be neglected in the adiabatic limit. For this reason QMC methodology becomes much simpler in this case and can be efficiently performed to obtain the relevant quantities in real time. In this section, we first derive the relevant equations and then present selected results for $C_{jj}(t)$ and $\mathcal{D}(t)$ in the adiabatic limit.

The Holstein Hamiltonian in this limit takes the form

$$H = \sum_{ij} h_{ij}(\{q\}) c_i^\dagger c_j + \sum_i \frac{1}{2} m \omega_0^2 q_i^2, \quad (\text{S32})$$

where

$$h_{ij}(\{q\}) = -t_0(\delta_{i,j+1} + \delta_{i,j-1}) + g\sqrt{2m\omega_0} q_i \delta_{ij}. \quad (\text{S33})$$

The operator c_i is the electron annihilation operator at site i , q_i is the coordinate of the phonon at site i , m is the oscillator mass, the symbol $\{q\}$ denotes all phonon coordinates, while phonon momenta p_i and the corresponding kinetic energy $\frac{p_i^2}{2m}$ were neglected. With the substitution of variables $x_i = q_i \omega_0 \sqrt{m}$, the Hamiltonian reduces to

$$H = \sum_{ij} h_{ij}(\{x\}) c_i^\dagger c_j + \sum_i \frac{1}{2} q_i^2, \quad (\text{S34})$$

with

$$h_{ij}(\{x\}) = -t_0(\delta_{i,j+1} + \delta_{i,j-1}) + 2\sqrt{\lambda t_0} q_i \delta_{ij}. \quad (\text{S35})$$

We evaluate the correlation function [\[see Eq. \(10\) of the main paper\]](#)

$$C_{jj}(t) = \frac{\text{Tr}(e^{-z_1 H} j e^{-z_2 H} j)}{\text{Tr} e^{-\beta H}} \quad (\text{S36})$$

(with $z_1 = \beta - it$, $z_2 = it$) by expressing the trace in the basis $|\{x\}n_{\{x\}}\rangle$, where $|n_{\{x\}}\rangle$ are the eigenstates of $h(\{x\})$ with phonon coordinates $\{x\}$ treated as classical variables. The matrix element of the Hamiltonian in this basis reads

$$\langle \{x\}n_{\{x\}} | H | \{y\}m_{\{y\}} \rangle = \delta(\{x\} - \{y\}) \delta_{mn} \left[\varepsilon_m(\{x\}) + \sum_i \frac{1}{2} x_i^2 \right], \quad (\text{S37})$$

where $\varepsilon_m(\{x\})$ are the eigenvalues of $h(\{x\})$. Consequently, we find

$$\langle \{x\}n_{\{x\}} | e^{-zH} | \{y\}m_{\{y\}} \rangle = \delta(\{x\} - \{y\}) \delta_{mn} e^{-z[\varepsilon_m(\{x\}) + \sum_i \frac{1}{2} x_i^2]}. \quad (\text{S38})$$

The trace in the numerator in Eq. (S36) reads

$$\text{Tr}(e^{-z_1 H} j e^{-z_2 H} j) = \int d\{x\} \sum_{m_{\{x\}}} \langle \{x\}m_{\{x\}} | e^{-z_1 H} j e^{-z_2 H} j | \{x\}m_{\{x\}} \rangle \quad (\text{S39})$$

which leads to

$$\text{Tr}(e^{-z_1 H} j e^{-z_2 H} j) = \int d\{x\} \sum_{m_{\{x\}} n_{\{x\}}} \langle \{x\}m_{\{x\}} | e^{-z_1 H} j | \{x\}n_{\{x\}} \rangle \langle \{x\}n_{\{x\}} | e^{-z_2 H} j | \{x\}m_{\{x\}} \rangle \quad (\text{S40})$$

and eventually

$$\begin{aligned} \text{Tr}(e^{-z_1 H} j e^{-z_2 H} j) &= \int d\{x\} e^{-\beta \sum_i \frac{1}{2} x_i^2} \sum_{m_{\{x\}} n_{\{x\}}} e^{-\beta \varepsilon_{m_{\{x\}}}} e^{it(\varepsilon_{m_{\{x\}}} - \varepsilon_{n_{\{x\}}})} \times \\ &\quad \langle m_{\{x\}} | j | n_{\{x\}} \rangle \langle n_{\{x\}} | j | m_{\{x\}} \rangle, \end{aligned} \quad (\text{S41})$$

as well as

$$\text{Tr}(e^{-\beta H}) = \int d\{x\} e^{-\beta \sum_i \frac{1}{2} x_i^2} \sum_{m_{\{x\}}} e^{-\beta \varepsilon_{m_{\{x\}}}}. \quad (\text{S42})$$

The correlation function given in Eq. (S36) can then be evaluated by sampling the phonon coordinates as Gaussians with standard deviation $\sigma^2 = \frac{1}{\beta}$ and performing the summation of the terms in the numerator and denominator. These summations are much less demanding than the summations in full Monte Carlo simulations because the number of phonon coordinates in this case is equal to the number of sites, while in full Monte Carlo simulations it is equal to the number of sites times the number of timesteps. The summations in Eqs. (S41) and (S42) can be interpreted as averages over classical phonon coordinates $\{x\}$. One should, however, note that the assumption of classical phonons was not introduced in the derivation. It is the neglect of phonon momentum that led to the expression which can be interpreted this way.

Next, we also give expression for the quantities $\langle N_e \rangle_K$, $\mathcal{G}^<(k, t)$ and $\mathcal{G}^>(k, t)$ which are needed to evaluate $C_{jj}^{\text{bbl}}(t)$ in accordance with [Eq. \(17\) of the main paper](#). We obtain

$$\mathcal{G}^>(k, t) = -ie^{i\mu_F t} \frac{\int d\{x\} e^{-\beta \sum_i \frac{1}{2} x_i^2} \sum_{m_{\{x\}}} e^{-i\varepsilon_{m_{\{x\}} t} |c_{mk}(\{x\})|^2}}{\int d\{x\} e^{-\beta \sum_i \frac{1}{2} x_i^2}}, \quad (\text{S43})$$

$$\mathcal{G}^<(k, t) = ie^{(\beta+it)\mu_F} \frac{\int d\{x\} e^{-\beta \sum_i \frac{1}{2} x_i^2} \sum_{m_{\{x\}}} e^{-(\beta+it)\varepsilon_{m_{\{x\}}} |c_{mk}(\{x\})|^2}}{\int d\{x\} e^{-\beta \sum_i \frac{1}{2} m\omega_0^2 x_i^2}}, \quad (\text{S44})$$

$$\langle N_e \rangle_K = e^{\beta\mu_F} \frac{\int d\{x\} e^{-\beta \sum_i \frac{1}{2} x_i^2} \sum_{m_{\{x\}}} e^{-\beta\varepsilon_{m_{\{x\}}}}}{\int d\{x\} e^{-\beta \sum_i \frac{1}{2} x_i^2}}, \quad (\text{S45})$$

where $c_{mk}(\{x\})$ is the overlap of the electronic state of momentum $|k\rangle$ and the electronic state $|m_{\{x\}}\rangle$ given as $c_{mk}(\{x\}) = \langle k | m_{\{x\}} \rangle$.

In Fig. S4 we present $C_{jj}(t)$ and $\mathcal{D}(t)$ for two parameters sets ($\lambda = \frac{1}{2}$, $T = 1$, $t_0 = 1$) and ($\lambda = 1$, $T = 2$, $t_0 = 1$). The numerically exact results obtained using HEOM are presented, as well as the results in the adiabatic limit obtained as described in this section. As expected, the exact results for $\omega_0 = 1/3$ are closer to the adiabatic limit results than the exact results for $\omega_0 = 1$. Nevertheless, both of these sets of results are still quite far from the adiabatic limit results. As discussed in the main paper, this is consistent with the fact that vertex corrections for these parameter sets are not very strong. We also present the bubble approximation results in the adiabatic limit. These results which yield a non-zero mobility strongly differ from the exact results which give a zero mobility, in accordance with expectations.

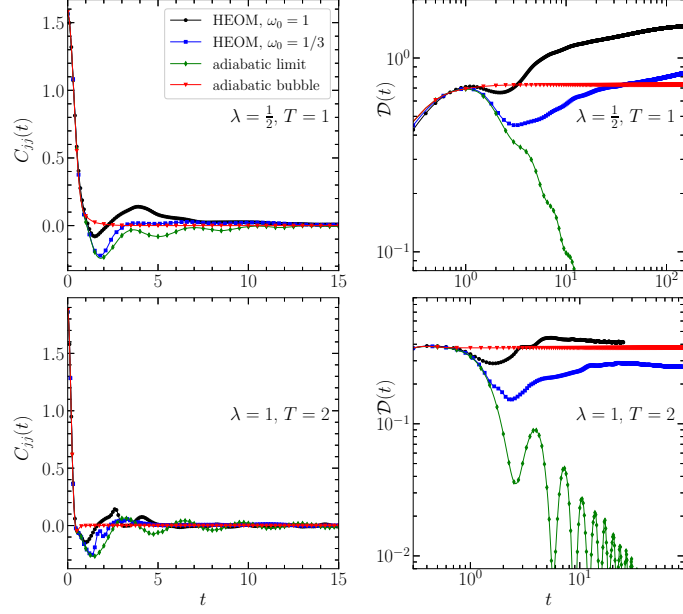


FIG. S4. The current-current correlation function $C_{jj}(t)$ and the diffusion constant $\mathcal{D}(t)$ for two parameters sets ($\lambda = \frac{1}{2}$, $T = 1$) and ($\lambda = 1$, $T = 2$) ($t_0 = 1$ in both cases). The results labeled as 'HEOM' denote the numerically exact results obtained using the hierarchical equations of motion method for two values of phonon frequencies $\omega_0 = 1$ and $\omega_0 = 1/3$, the results labeled as 'adiabatic limit' denoted the results obtained in the adiabatic limit using the methodology described in this section, while the results labeled as 'adiabatic bubble' are the results obtained with the bubble approximation in the adiabatic limit.

SVI. COMPARISON OF THE RESULTS FOR DC MOBILITY OBTAINED FROM REAL-TIME AND IMAGINARY-TIME COMPUTATIONS

Figure S5 compares some of our HEOM and DMFT results for μ_{dc} , both of which follow from real-axis computations, with the corresponding results of Ref. 5, which were extracted from imaginary-axis data using numerical analytical continuation. While all the results are virtually the same in the weak-interaction regime $\lambda = 1/100$, the results of Ref. 5 seem to severely underestimate μ_{dc} (by approximately an order of magnitude) in the intermediate-interaction regime $\lambda = 1/2$.

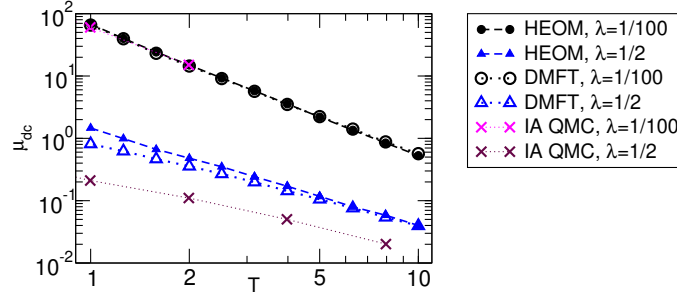


FIG. S5. Comparison of HEOM (full symbols), DMFT (empty symbols), and imaginary-axis QMC (crosses) results of Ref. 5 for the temperature dependent dc mobility. The model parameters are $t_0 = \omega_0 = 1$ and $\lambda = 1/100$ and $1/2$.

-
- [1] V. Janković, Holstein polaron transport from numerically “exact” real-time quantum dynamics simulations, *J. Chem. Phys.* **159**, 094113 (2023).
 - [2] V. Janković and N. Vukmirović, Spectral and thermodynamic properties of the Holstein polaron: Hierarchical equations of motion approach, *Phys. Rev. B* **105**, 054311 (2022).
 - [3] D. M. Wilkins and N. S. Dattani, Why quantum coherence is not important in the Fenna-Matthews-Olsen complex, *J. Chem. Theory Comput.* **11**, 3411 (2015).
 - [4] W. H. Press, S. A. Teukolsky, W. T. Vetterling, and B. P. Flannery, *Numerical Recipes in C*, 2nd ed. (Cambridge University Press, Cambridge, USA, 1992).
 - [5] A. S. Mishchenko, N. Nagaosa, G. De Filippis, A. de Candia, and V. Cataudella, Mobility of Holstein polaron at finite temperature: An unbiased approach, *Phys. Rev. Lett.* **114**, 146401 (2015).